JOURNAL OF MATERIALS SCIENCE **36** (2001) 5105–5113

Sub-micron sized Al_2TiO_5 powders prepared by high-energy ball milling

R. URIBE, C. BAUDÍN
Instituto de Cerámica y Vidrio (CSIC), Arganda del Rey, Madrid, Spain 28500
L. MAZEROLLES, D. MICHEL
Centre d'Etudes de Chimie Métallurgique, CNRS UPR 2801, 94407 Vitry Cedex, France

High energy ball milling to obtain ultrafine aluminium titanate particles has been investigated. Tempered steel has been selected as material for the containers and balls because the desirable properties of aluminium titanate are not degraded by small amounts of Fe_2O_3. The starting powders have been milled during different periods (1–60 h) and the evolution of the morphology and crystallinity of the treated powders as well as the extent of contamination from the milling media have been characterised. Different experimental techniques, X-ray diffraction, BET-analysis, chemical analysis, scanning electron microscopy and low and high resolution transmission electron microscopy have been used. High energy ball milling has been proved to be an efficient route to obtain submicron sized (50–100 nm) aluminium titanate powders, but further milling of the powders is accompanied by contamination from the milling media and the formation of hard agglomerates.

1. Introduction

Ceramic materials based on aluminium titanate, Al_2TiO_5, have many possibilities for technological applications related to their excellent thermal properties. The stable phase at room temperature, β-Al_2TiO_5, has been the subject of many studies, due to its very low thermal expansion coefficient ($0.2–1.0 \times 10^{-6}$ °C^{-1}), low thermal conductivity (0.9–1.5 $Wm^{-1}K^{-1}$) and excellent thermal shock resistance [1–9]. The crystal structure of aluminium titanate is the pseudobrookite type [10] with a theorical density of 3.70 g/cm^3. This material is conventionally prepared by reaction sintering of α-Al_2O_3 and TiO_2-rutile with densities of 3.99 and 4.25 g/cm^3, respectively. Therefore, the reaction described by Equation 1 is accompanied by a 11% molar volume increase.

$$\alpha\text{-}Al_2O_3 + TiO_2\text{-rutile} \rightarrow \beta Al_2TiO_5 \qquad (1)$$

The kinetics of aluminium titanate formation from the binary oxides has been carefully investigated by Freudenberg and Mocellin [6, 7]. Two different reaction stages were identified during isothermal treatment around 1300°C. The initial stage was characterized by the rapid growth of a limited number of large aluminium titanate cells, 10 to 100 μm in size, into a virtually unreacted powder mixture (≈40 wt%) consisting of micrometer-size particles. The diffusion controlled final reaction stage corresponds to the elimination of Al_2O_3 and TiO_2 dispersoids trapped during the initial growth of aluminium titanate cells. The rate of aluminium titanate formation in this stage is 3 to 4 orders of magnitude smaller than the initial aluminium titanate cell growth rate.

β-Al_2TiO_5 presents two important drawbacks that imply serious limitations for high-temperature applications. The first is the thermodynamic instability of this phase under 1280°C [11, 12], resulting in the decomposition of the material between this temperature and 750°C to form an Al_2O_3-TiO_2 mixture. This decomposition can be controlled by adding small amounts of chemical stabilizers, MgO and Fe_2O_3, which lead to the formation of pseudobrookite $Mg_xAl_{2(1-x)}Ti_{(1+x)}O_5$ and $Fe_{2x}Al_{2(1-x)}TiO_5$ solid solutions during sintering [4, 5, 11, 13]. The second problem is related to the extensive microcraking that takes place in the materials during cooling from the sintering temperature due to the extreme thermal expansion anisotropy of aluminium titanate [14–19]. Microcracking is responsible for the low thermal expansion coefficient but also for a very low strength. The occurrence of microcracking is influenced by the microstructure of the materials and, in particular, by the grain size. The critical Al_2TiO_5 grain size for spontaneous fracture has been estimated as 1 to 2 μm [15] or 2.5 μm [18]. Consequently, a fine grained microstructure is required for monolithic aluminium titanate materials to have mechanical stability.

Several methods have been proposed for the synthesis of aluminium titanate [6–8, 20–23], which include conventional processing of oxides, hydrothermal, stepwise hydration of titanium alkoxide in alumina dispersion, gas-phase pyrolysis, and sol-gel techniques. In general, exaggerated grain growth and subsequent cracking occur in aluminium titanate materials obtained directly by the reaction sintering of alumina and titania powders. Moreover, these materials present high levels of porosity because densification during the thermal

treatment is impeded by the growth of the reacted aluminium titanate cells. The seeding of the starting monophasic and diphasic gels by $MgTi_2O_5$ has been proposed as a way to enhance densification of the materials [21].

A possibility for the fabrication of fine grained aluminium titanate materials is the conventional sintering of ultrafine and already reacted powders. In a previous work [23], the formation of aluminium titanate from equimolar mixtures of high purity and fine grained ($d_{50} < 0.5\,\mu$m) Al_2O_3 and TiO_2 powders and the influence of the microstructure of the obtained compacts on the milling efficiency, to obtain fine aluminium titanate powders was studied. Different thermal treatments with maximum temperatures between 1350 and 1650°C were considered and their influence on the degree of reaction and the cell size of Al_2TiO_5 was established. The results showed that the degree of reaction changes from practically zero at 1350°C to complete reaction at 1650°C, except for the presence of some isolated alumina particles. Attrition milling efficiency as a function of the thermal treatment was studied on the materials that presented the highest degree of reaction. The minimum average particle size that it was possible to obtain, without extensive agglomeration of the powders during milling, was 0.5 μm.

High energy ball-milling has been extensively used for the synthesis of metallic or intermetallic compounds, carbides, silicides, nitrides and oxides [24]. This technique is also applied for preparing ultra-fine powders with specific structure or composition [25]. In this work, the possibility of obtaining ultrafine aluminium titanate particles by high energy ball milling has been investigated. Tempered steel has been selected as material for the containers and balls because Fe_2O_3, which form solid solution with aluminium titanate in amounts up to 8 wt%, is an aluminium titanate stabiliser [5] and, therefore, iron contamination from the milling media is not expected to degrade the desirable properties of aluminium titanate.

2. Experimental procedure

The β-Al_2TiO_5 starting powder was obtained by reaction of high-purity commercial powders of alumina (>99.9 wt%) and titania (>99.5 wt%) following the method described elsewhere [23].

The high-energy milling has been performed in a planetary ball-mill allowing independent control of rotation speed of the disk (Ω) and the vial holders (ω) [26]. The radius of the disk and the internal radius of vials are 75 and 20 mm, respectively, which are typical conventional values (Pulverisette P7/2, Fristsh GmbH, Idar-Oberstein, Germany). The Ω rotation is chosen to be clockwise and ω to be counterclockwise. An electronic tachometer controls the effective rotation speed. In the present work, the Ω and ω values were 500 and 250 rpm, respectively. Two tempered-steel containers of 90-ml capacity loaded with five steel balls (diameter 15 mm, mass 14 g) were used as milling media.

Ten grams of the starting powder were introduced into each container for milling. Portions of the milled powders were extracted from the containers after different milling times (1–60 h) and characterised.

X-ray diffractometry (XRD; PW 1830 Philips, Eindhoven, The Netherlands) has been performed using the filtered K_α radiation of a cobalt target. Spectra were recorded from 10° to 140° in 2θ angle with a 10-s counting for each 0.025° step.

Results were analyzed with an automatic powder diffraction software (APD, Philips, Eindhoven, The Netherlands) allowing the determination of the position and intensity of diffraction lines, as well as line profile analysis by fit to a Voigt function. Crystallite size and lattice strain have been estimated assuming that the Lorentzian and Gaussian characters of the line broadening are associated to crystallite size and lattice strain effects, respectively. The experimental profiles have been corrected from $K_{\alpha 2}$ radiation and Lorentz polarization, and the instrumental profile measured on a well crystallized were analyzed for the "single line method" using the analysis of Fourier coefficients [25]. The diffraction lines of β-Al_2TiO_5 have been identified after refinement of lattice constants by comparison with the 26-0040 ASTM card index.

The specific surface areas of the milled powders have been determined using a series surface area and pore size analyzers (SA 3100 Coulter, Coulter Corporation, EE UU). The BET (Brunauer, Emmett and Teller) surface area was calculated from a multilayer adsorption theory using nitrogen adsorption - desorption at 350°C.

The amounts of iron have been determined via chemical analysis by inductively couple plasma atomic emission spectrometry (ICP-AES; Spectrometer Iris Advantage, Thermo Jarrell Ash, EE UU), and recalculated as Fe_2O_3. Scanning electron microscopy at low voltage (SEM, 1 kV, DSM 982 LEO, Germany) in ln Lens mode, low and high resolution transmission electron microscopies (TEM, 125 kV, HITACHI, H-7000, Japan; HRTEM, 200 kV, 002B, TOPCON, Japan) have been used to analyse the morphology of the powders. High resolution microscopy was used for imaging the internal structure of nanoparticles at atomic scale and to reveal eventual defects after numerical treatment (Bragg filtering by Fourier transform). TEM observations were carried on powders dispersed by an ultrasonic treatment in water and deposited on a holey carbon grid. HRTEM observations were carried on powders dispersed in ethanol and deposited on a holey carbon grid.

3. Results and discussion

Fig. 1 shows the evolution of the powder crystallinity as a function of milling time. The broadening of β-Al_2TiO_5 peaks after 2 hours of milling is apparent. A broad line at interplanar distance 0.20 nm ($2\theta = 52.28$), which corresponds to the strongest 110 line of α-type iron is observed clearly from 8 h milling, and corresponds to contamination from the milling medium. The intensity of this line increased with the milling time in agreement with the amount of iron detected by chemical analysis (Table I). The sharp increase in the amount of iron from 4 to 8 h milling was proved to be consistent for different batches of powders. From 8 h, the extent

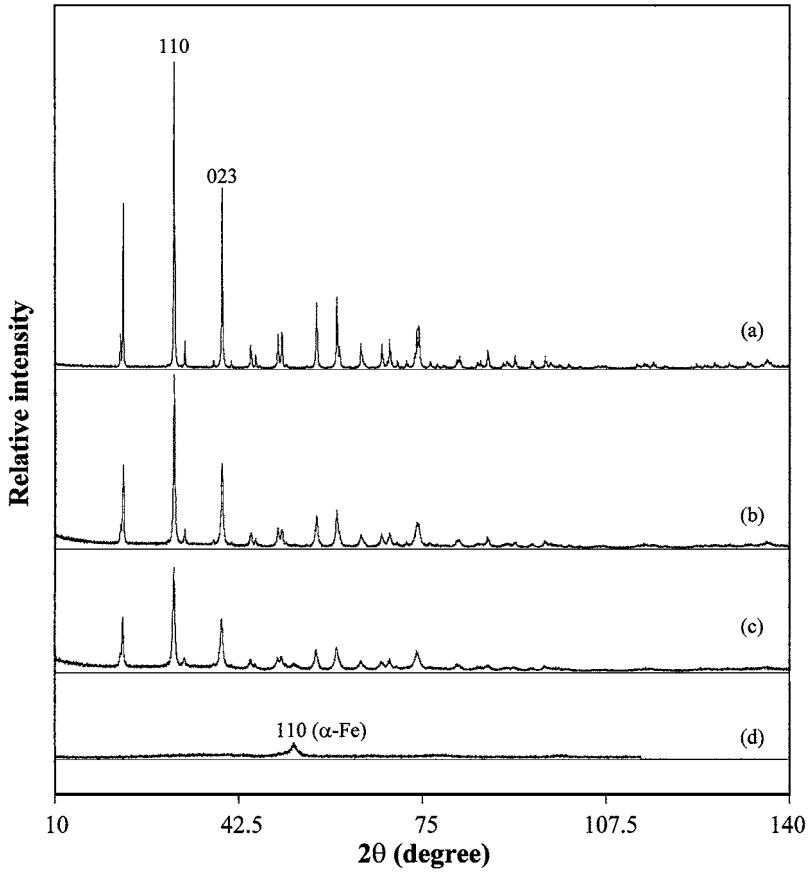

Figure 1 XRD patterns of Al_2TiO_5 powders obtained after high-energy milling ($\Omega = 500$ rpm, $\omega = 250$ rpm) for: (a) 0 h; (b) 4 h; (c) 8 h; (d) 40 h.

of contamination increases steadily with milling time (Table I).

In order to estimate the effect of milling on crystallite size and lattice distortion the 110 and 023 XRD lines profiles were fitted to Voigt curves. These two lines were chosen because the other lines were not sufficiently intense or overlapped. The results given in Table II indicate that both particle size and lattice strain contribute significantly to line broadening. The coherence length varies from ≈120 nm to ≈20 nm and the lattice strain from ≈0.2% to ≈0.9%, for the powders milled during 1 h and 40 h, respectively. These lattice strain values would indicate that the milling has introduced a noticeable rate of crystal defects in the formed nanocrystals.

TABLE I Chemical analysis results for Fe_2O_3 contamination as a function of the milling time of the Al_2TiO_5 powders

Milling time (h)	Fe_2O_3 (wt%)
0	0.04
2	0.21
4	0.8 ± 0.3
8	6.2 ± 0.4
14	6.1 ± 0.5
24	8.30
40	12.30
60	13.00

TABLE II XRD line width analysis as a function of the milling time of the Al_2TiO_5 powders

	Coherence length (nm)		Lattice strain (%)	
	Diffraction lines (*hkl*)		Diffraction lines (*hkl*)	
Milling time (h)	110	023	110	023
1	130 ± 10	100 ± 10	0.20 ± 0.01	0.16 ± 0.01
2	110 ± 10	90 ± 8	0.14 ± 0.02	0.19 ± 0.01
4	65 ± 5	45 ± 4	0.28 ± 0.01	0.32 ± 0.02
8	32 ± 3	25 ± 4	0.52 ± 0.02	0.54 ± 0.03
40	30 ± 3	10 ± 2	0.86 ± 0.08	1.00 ± 0.05

Calculations of the particle size, d, from the BET specific surface area, SA_{BET}, and the theoretical density, ρ_{th}, of aluminium titanate assuming spherical particles using:

$$d = 6(\rho_{th} SA_{BET})^{-1} \quad (2)$$

lead to much larger values (205, 294, 444, 1060, nm for powders milled 2, 4, 8 and 40 h respectively) than those reported in Table II, and only the values corresponding to 2 and 4 h milling were smaller than the values corresponding to the starting powder. This result might indicate that the agglomeration of the powders takes place during milling as discussed below.

The evolution of powder morphology with milling time is showed in Figs 2 and 3. Low magnification SEM micrographs (Fig. 2) show that in the powders milled up to 8 h a mixture of micro and nanosized particles is present (Fig. 2a–c), whereas practically no independent nanoparticles can be observed in the powder milled during 40 h (Fig. 2d). Larger magnification SEM micrographs (Fig. 3) show the substructure of the micro-sized particles. For short milling times (Fig. 3a), these particles are the original aluminium titanate ones and the erosive effect of milling is observed on their surface as erosion tracks and detached independent

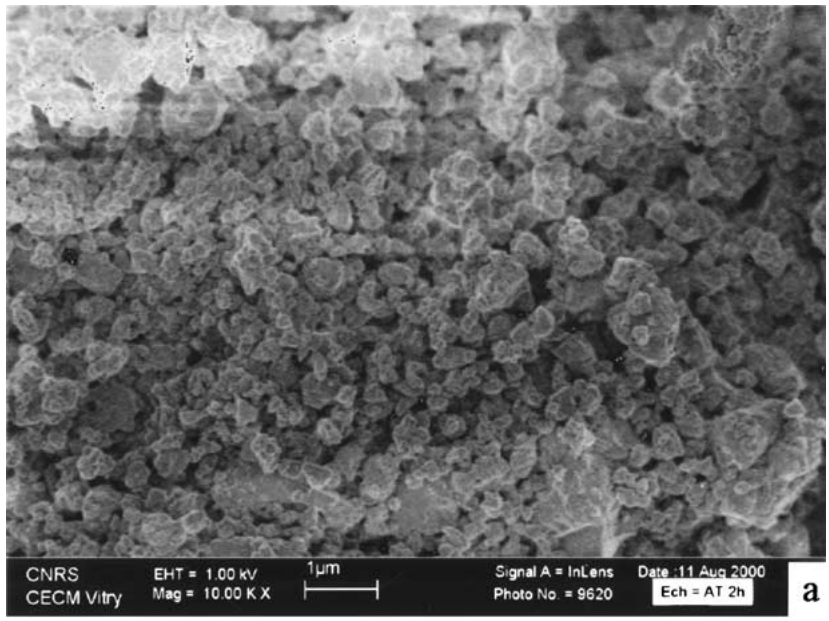

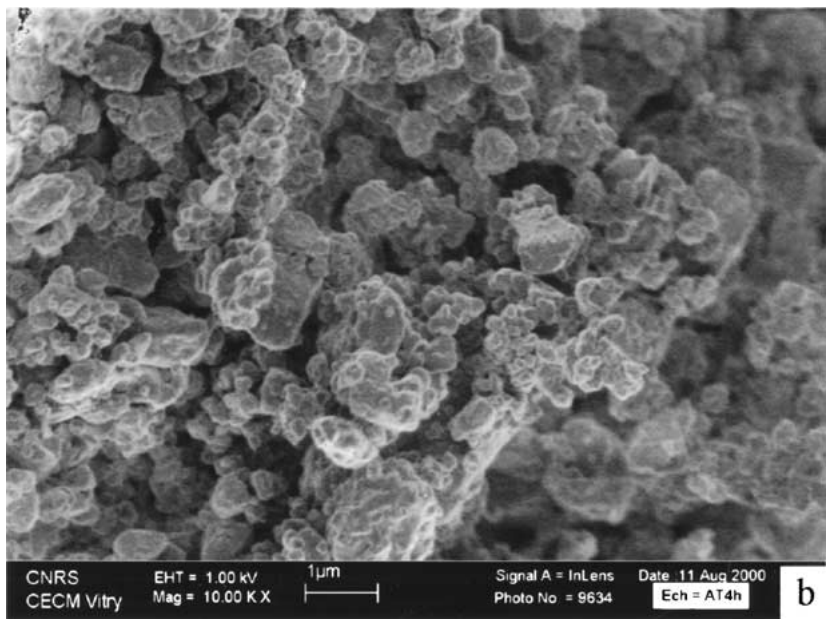

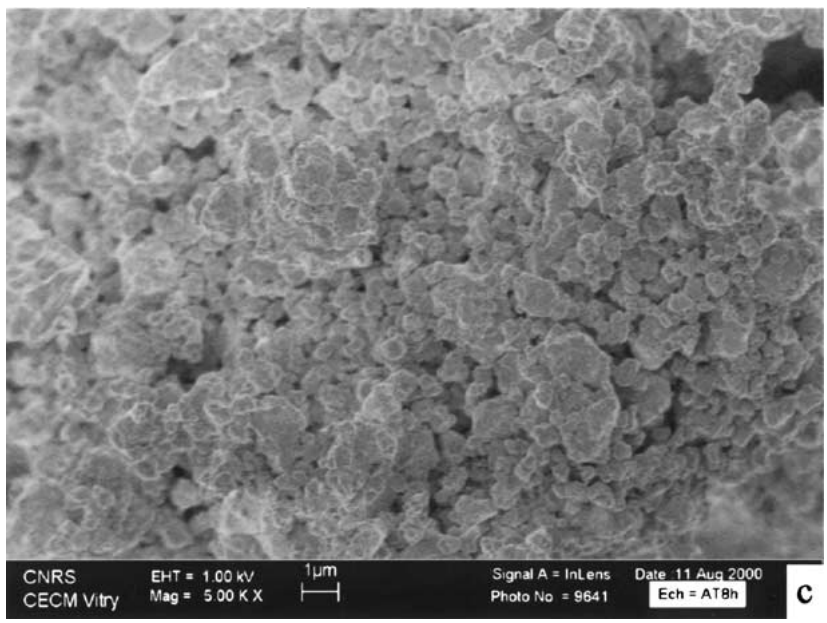

Figure 2 Low magnification SEM micrographs (ln Lens image) of Al_2TiO_5 powders after high-energy milling ($\Omega = 500$ rpm, $\omega = 250$ rpm) for: (a) 0 h; (b) 4 h; (c) 8 h; (d) 40 h. (*Continued*.)

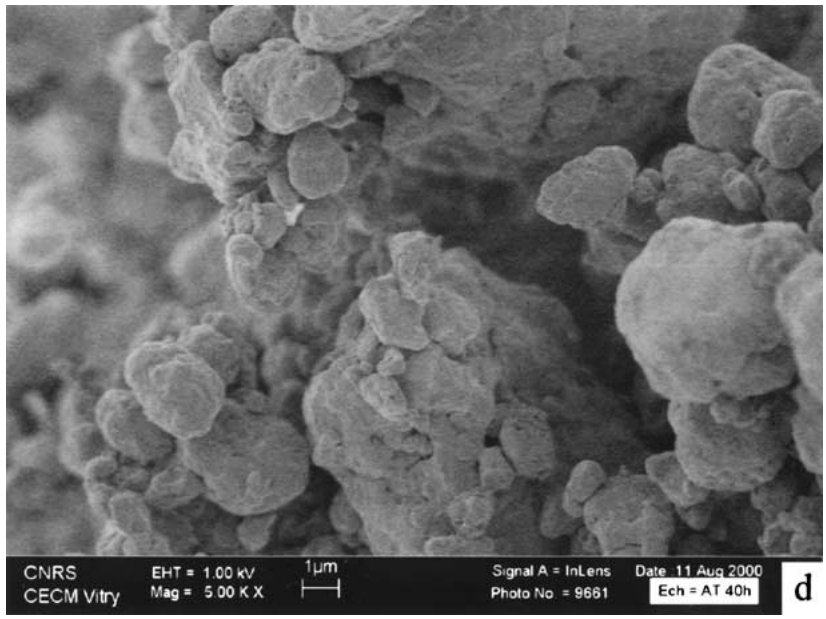

Figure 2 (*Continued*.)

nanoparticles. The specific surface area of the mixture of eroded and nanosized particles is lower than that of the original ones (Table III). The amount of nanoparticles increase with milling time, but they are forming agglomerates in the powder milled for 4 and 8 h (Fig. 3b and c). These nanoparticles cannot be distinguished in the powder milled for 40 h (Fig. 3d), in which case the surface of the micro-sized particles appears to be continuous. Agglomeration of the powders from 4 hours milling time is accompanied by the decrease of specific surface area (Table III).

TABLE III BET specific surface area as a function of the milling time of the Al_2TiO_5 powders

Milling time (h)	Specific surface area (m^2/g)
0	5.14
2	7.91
4	5.51
8	3.65
40	1.53

TEM examination reveals that these agglomerate particles are, in fact, aggregates of aluminium titanate nanocrystals. The examination of deagglomerated powders (Fig. 4a) shows that the crystallite sizes are 100 and 50 nm for 2 and 4 hours milling, respectively (Fig. 4b and c). These values are in good agreement with the mean size particle estimated from the width of XRD lines. It was not possible to separate the agglomerates formed in the powders milled for more than 4 hours into individual particles. This fact indicates that the agglomerates formed for long milling times (>4 h) are hard agglomerates.

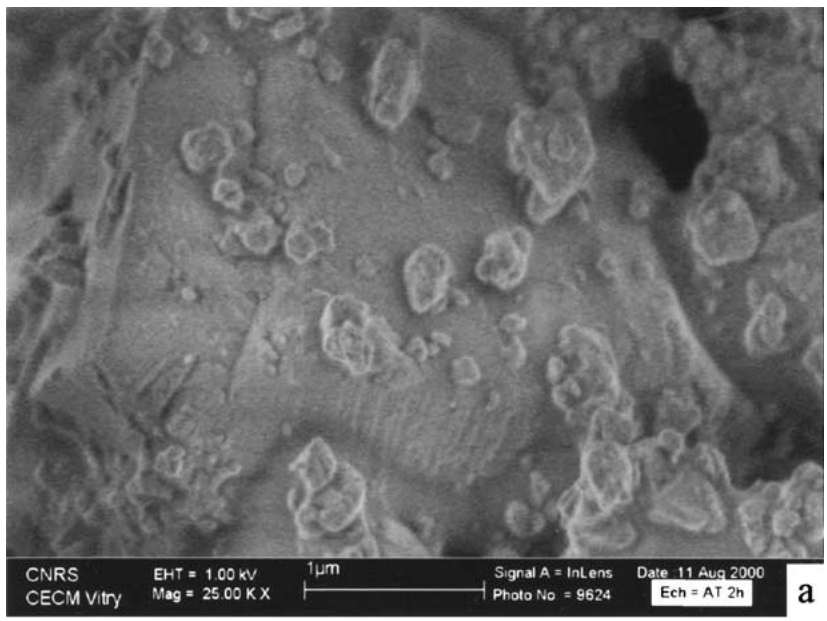

Figure 3 Higher magnification SEM micrographs (ln Lens image) of Al_2TiO_5 powders after high-energy milling ($\Omega = 500$ rpm, $\omega = 250$ rpm) for: (a) 0 h; (b) 4 h; (c) 8 h; (d) 40 h. (*Continued*.)

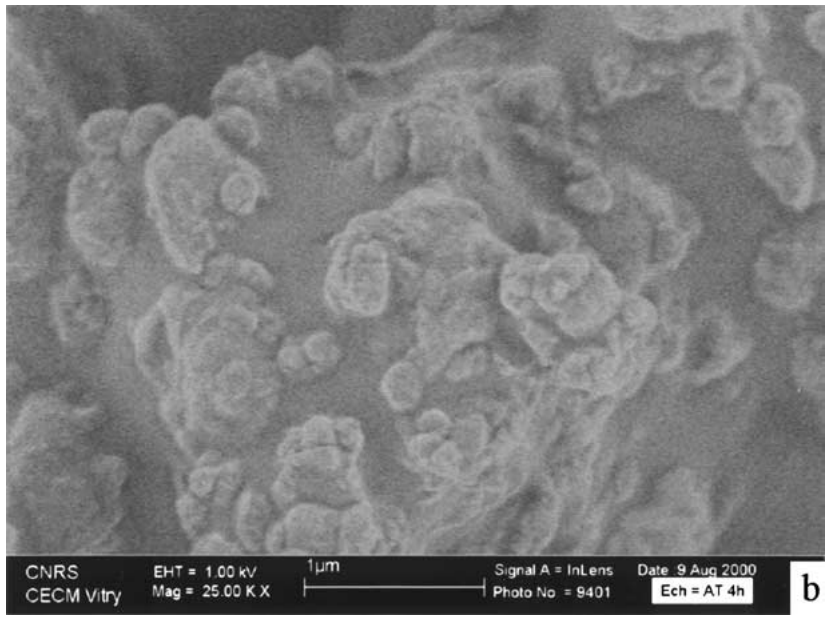

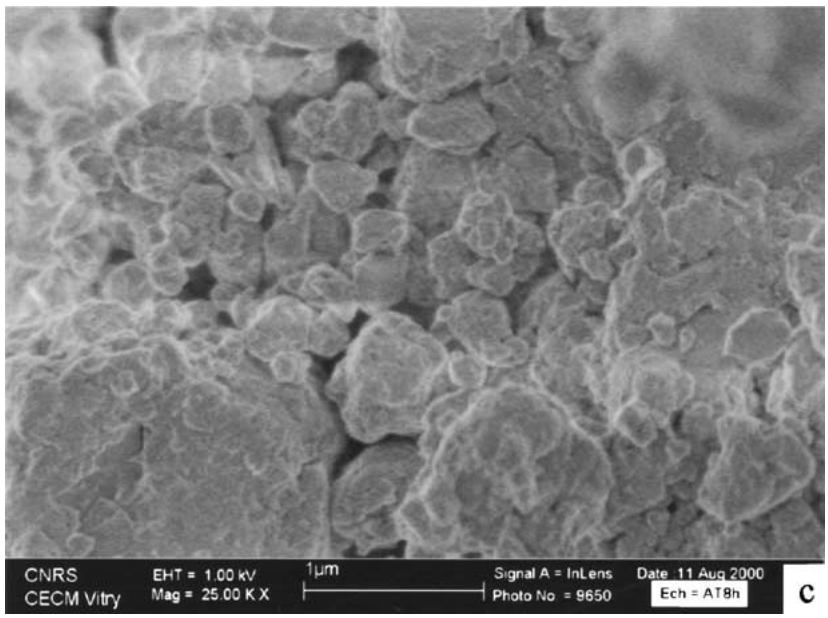

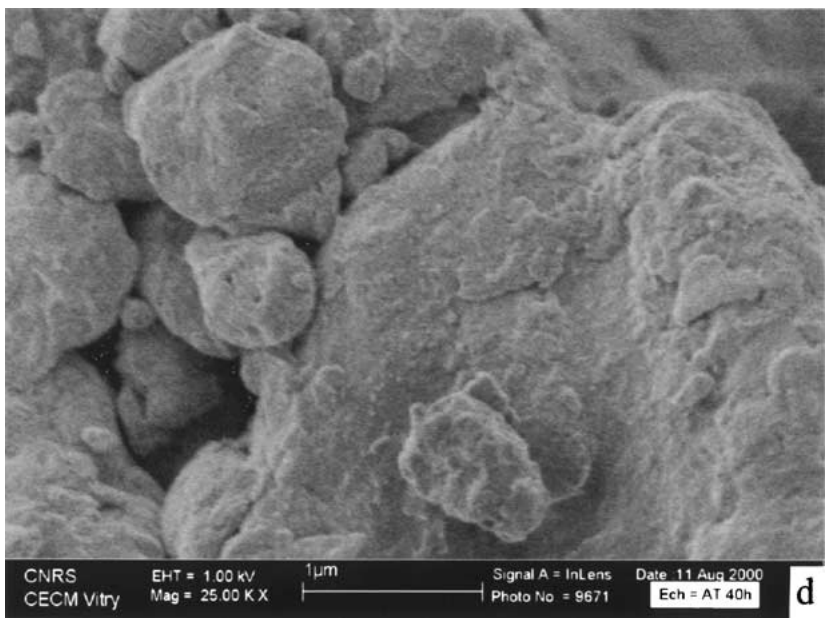

Figure 3 (*Continued.*)

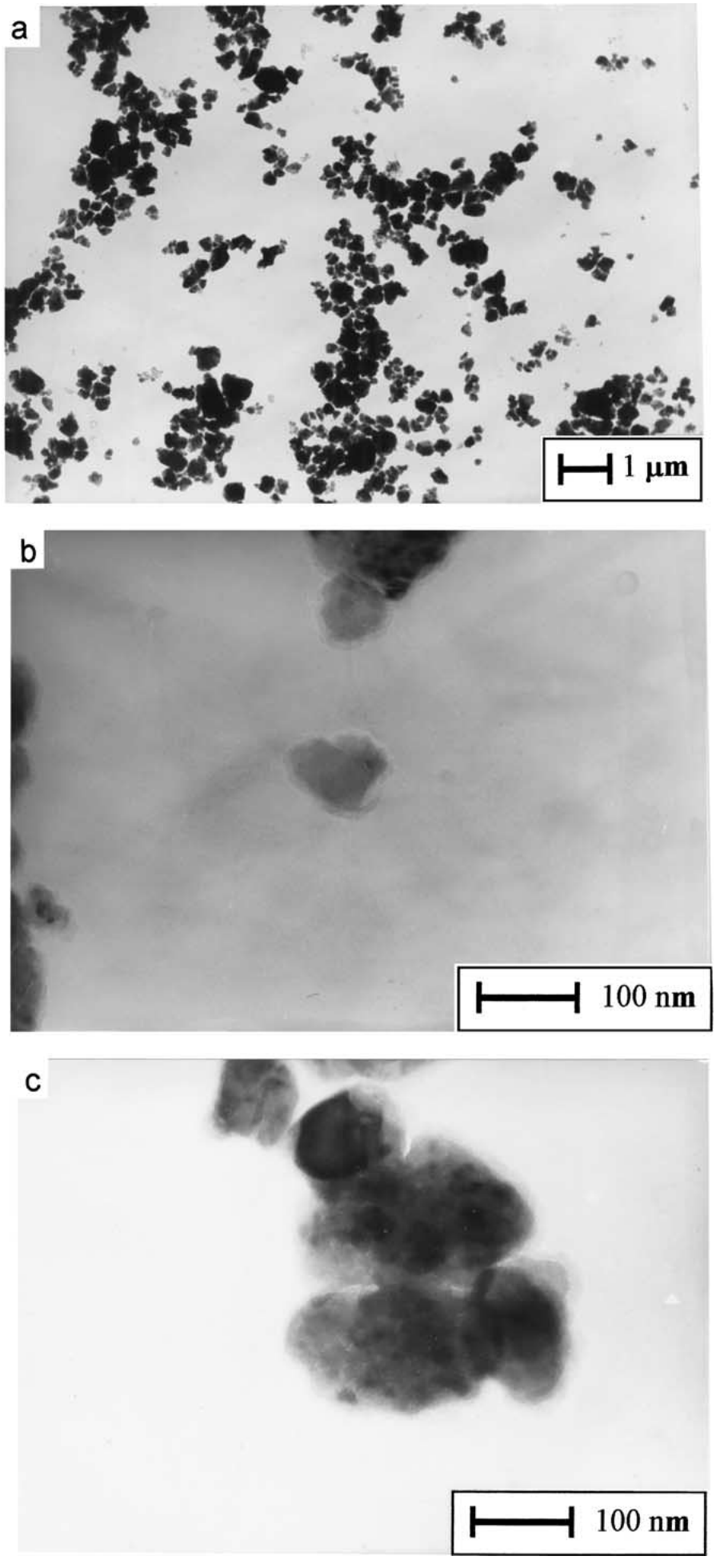

Figure 4 TEM micrographs of Al_2TiO_5 powders after high-energy milling ($\Omega = 500$ rpm, $\omega = 250$ rpm) for: (a) 2 h; (b) 2 h; (c) 4 h.

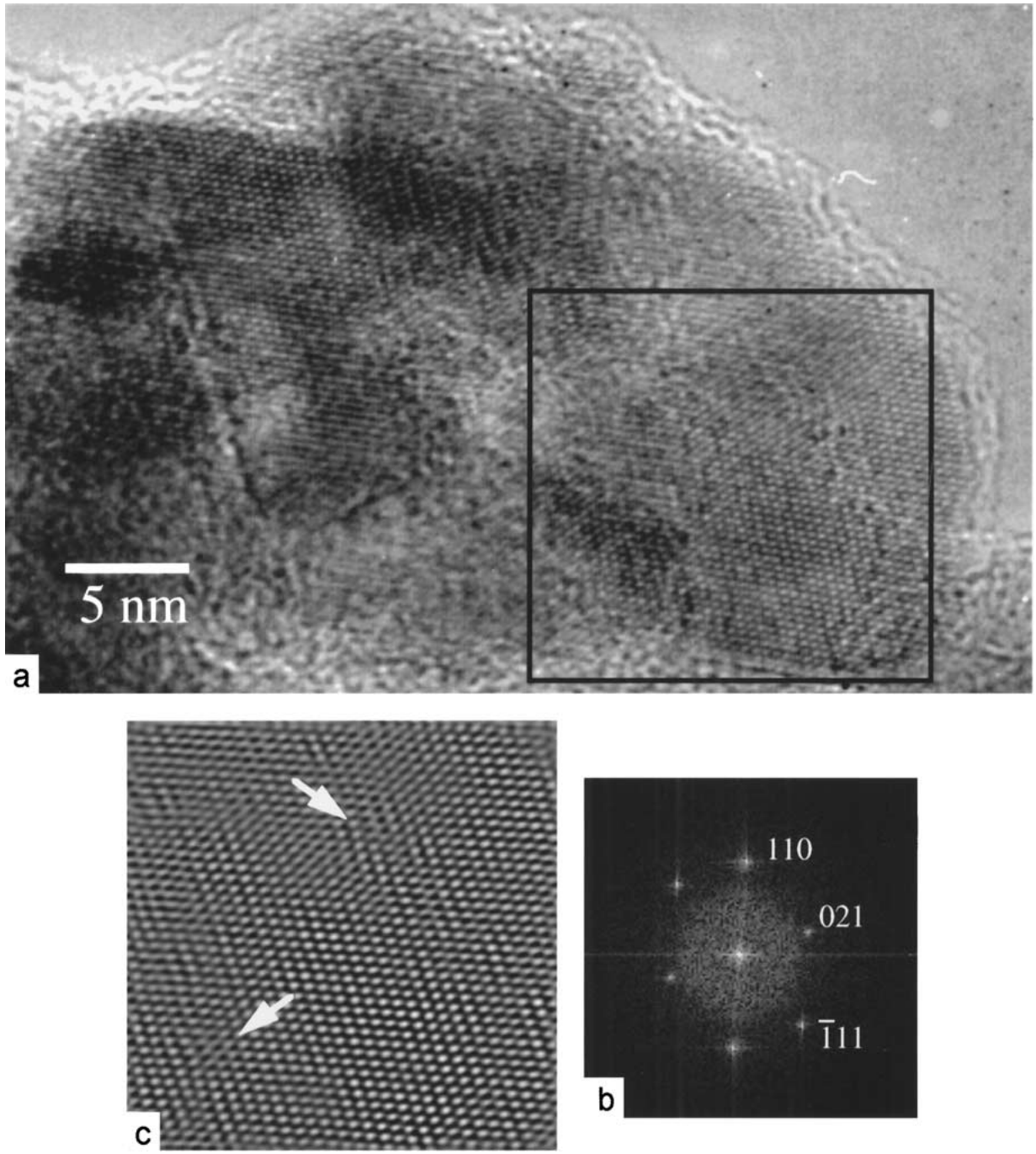

Figure 5 Internal structure of the sub-micron sized Al_2TiO_5 particles: (a) HRTEM image of a Al_2TiO_5 crystallite from the powder milled during 4 h; (b) Numerical diffraction (modulus of Fourier Transform) of the whole image; (c) Image reconstructed by inverse Fourier Transform of the inset zone. Defects indicated by arrows are revealed by Bragg filtering.

HRTEM was used to investigate the structure of the sub-micron sized particles. As an example obtained on the powder milled during 4 hours, Fig. 5 represents a HRTEM image of an aluminium titanate crystallite, oriented along the [1$\bar{1}$2] zone axis. This image has been filtered using Bragg filtering. The procedure to produce a Bragg filtered image from the digitised image, is to place a mask around the spots in the Fourier transform of the image (reciprocal space) and then to do the back-Fourier transform. The Fourier reconstruction of a part of the image, by this operation (Fig. 5c), shows the presence of crystallographic defects in this particle, in agreement with the lattice strain values determined for the milled powders (Table II). The streaks visible on the computed diffraction pattern, close to the Bragg spots, are not due to atomic displacements in the structure but an artefact coming from the small area selected for computing the Fourier transform.

4. Conclusions

High energy ball milling under the experimental conditions here described has proved to be an efficient method for obtaining submicron sized (50–100 nm) aluminium titanate powders. Such powders are obtained after 4 hour milling with a reasonably low iron contamination coming from the process. Further milling induces an amorphisation of the powders which is accompanied by extensive contamination of iron from the balls and the formation of hard agglomerates.

Acknowledgements

This work has been supported by CICYT MAT96-0408, CONICIT (Venezuela) and CNRS-CSIC: project N° 7948 (France): project N° 2000FR0004 (Spain). The authors wish to thank Jean-Louis Pastol for SEM studies.

References

1. H. A. J. THOMAS and R. STEVENS, *Brit. Ceram. Trans. J.* **88** (1989) 144.
2. *Idem.*, *ibid.* **88** (1989) 184.
3. F. J. PARKER, *J. Amer. Ceram. Soc.* **73** (1990) 929.
4. H. WOHLFROMM, J. S. MOYA and P. PENA, *J. Mater. Sci.* **25** (1990) 3753.
5. G. TILLOCA, *ibid.* **26** (1991) 2809.
6. B. FREUDENBERG and A. MOCELLIN, *J. Amer. Ceram. Soc.* **70**(1) (1987) 33.
7. *Idem.*, *ibid.* **71**(1) (1988) 22.
8. V. BUSCAGLIA, P. NANNI, G. BATTILANA, G. ALIPRANDI and C. CARRY, *J. Eur. Ceram. Soc.* **13** (1994) 411.
9. V. BUSCAGLIA, M. ALVAZZI, M. LEONI and C. BOTTINO, *J. Mater. Sci.* **31** (1996) 1715.
10. B. MOROSIN and R. LYNCH, *Acta Crystallogr. Sect B* **28** (1972) 1040.
11. M. ISHITSUKA, T. SATO, T. ENDO and M. SHIMADA, *J. Amer. Ceram. Soc.* **70** (1987) 69.
12. V. BUSCAGLIA and P. NANNI, *ibid.* **81**(10) (1998) 2645.
13. V. BUSCAGLIA, V. NANNI, M. ALVAZZI, M. LEONI and C. BOTTINO, *Adv. Sci. Technol.* **3c** (1995) 1867.
14. W. BUESSEM, N. THIELKE and R. SARAKAUSKAS, *Ceram. Age.* **60** (1952) 38.
15. J. CLEVELAND and C. BRADT, *J. Amer. Ceram. Soc.* **61**(11) (1978) 478.
16. W. RICE and R. POHANCA, *ibid.* **62**(12) (1979) 559.
17. A. EVANS, *Acta Metall.* **29** (1981) 1695.
18. Y. OHYA, K. HAMANO and Z. NAKAGAWA, *Yogyo Kyokaishi* **91**(6) (1983) 289.
19. *Idem.*, *J. Amer. Ceram. Soc.* **70**(8) (1987) C-184.
20. H. A. J. THOMAS and R. STEVENS, *Brit. Ceram. Trans. J.* **88** (1989) 229.
21. A. PRASADARAO, U. SELVARAJ, S. KOMARNENI, A. BHALLA and R. ROY, *J. Amer. Ceram. Soc.* **75**(6) (1992) 1529.
22. H. L. LEE and S. H. LEE, *J. Mater. Sci. Lett.* **13** (1994) 316.
23. R. URIBE and C. BAUDÍN, *Bol. Soc. Esp. Cerá m. Vidrio.* **39**(2) (2000) 221.
24. D. MICHEL, L. MAZERROLLES and E. GAFFET, *Third Euro-Ceramics* **1** (1993) 255.
25. D. MICHEL, F. FAUDOT, E. GAFFET and L. MAZERROLLES, *J. Amer. Ceram. Soc.* **76**(11) (1993) 2884.
26. E. GAFFET, *Mater. Sci. Eng.* **A132** (1991) 181.

Received 1 December 2000
and accepted 16 July 2001